Weierstraß–Institut
für Angewandte Analysis und Stochastik

im Forschungsverbund Berlin e.V.

Preprint ISSN 0946 – 8633

Dynamics of multi-section DFB semiconductor laser: traveling wave and mode approximation models

Mindaugas Radziunas[1,2] , Hans-Jürgen Wünsche[2]

submitted: 29 Jan 2002

[1] Weierstraß-Insitute für Angewandte Analysis und Stochastik, Mohrenstr. 39, 10117 Berlin, Germany
E-Mail: radziuna@wias-berlin.de

[2] Humboldt-Universität zu Berlin, Institut für Physik, Invalidenstr. 110, 10115 Berlin, Germany
E-Mail: wuensche@physik.hu-berlin.de

Preprint No. 713
Berlin 2002

1991 *Mathematics Subject Classification.* 78A60,35P10,37N20,37G35.

Key words and phrases. Traveling wave, mode approximation, modeling, bifurcation, multi-section DFB laser.

Edited by
Weierstraß–Institut für Angewandte Analysis und Stochastik (WIAS)
Mohrenstraße 39
D — 10117 Berlin
Germany

Fax: + 49 30 2044975
E-Mail (X.400): c=de;a=d400-gw;p=WIAS-BERLIN;s=preprint
E-Mail (Internet): preprint@wias-berlin.de
World Wide Web: http://www.wias-berlin.de/

Abstract

Nonlinear dynamical effects of a multi-section DFB semiconductor laser such as self-pulsations or hysteresis can be described by the traveling wave model. The present paper demonstrates that such a model can be effectively approximated by a low dimensional system of ordinary differential equations where only few dynamically varying longitudinal modes of optical field are taken into account. A bifurcation analysis of the reduced models allow us to identify the mechanisms of switching on and switching off of the self-pulsations by tuning model parameters. An explanation of hysteresis is given as well.

1 Introduction

Multi-section semiconductor lasers are of great interest in the process of developing all optical signal processing in optical communication systems. For example, high-frequency self-pulsations (SP) in three-section DFB lasers were successfully applied for all-optical clock recovery [1].

In designing lasers with prescribed dynamical behaviour, modelling plays a crucial role. There are many different models describing the photon and carrier behaviour inside semiconductor lasers, ranging from complex multidimensional partial differential equation models [2, 3] down to simple rate equation models where only temporal change of averaged photon and carrier densities are considered [4].

In order to keep everything as simple as possible but still to be able to resolve the multi-section structure of the considered devices, the present paper combines the traveling wave (TW) equation model with included influence of polarization and rate equations for the spatially averaged carrier densities inside each section [5, 6]. This partial differential equation model has only one spatial dimension what allows to compute the solutions in reasonable time. We have shown already in [5, 6, 7] that this model is able to recover such dynamical effects as SP, hysteresis and excitability demonstrated experimentally.

Simple computations of the model equations by changing one or another parameter can give only partial insight into the dynamics of semiconductor lasers. When optimizing design parameters to have a required robust behaviour of the laser, a much deeper understanding of the bifurcations separating different dynamical regimes is desired. The methods to analyze stability of the stationary states of the TW model were discussed in [8, 9]. But the study of nonstationary solutions requires more advanced tools, allowing to make a full bifurcation analysis of the TW model.

Well developed path-following and bifurcation analysis tools [10] are mainly suited to analyze dynamics of nonlinear ordinary differential equations and still cannot be directly applied to the TW model. In order to analyze our model, we approximate it with a system of ordinary differential equations, where only few most important dynamically varying longitudinal modes are taken into account [11, 12]. After determining the number of necessary modes and confirming the precision of mode approximation (MA) equations, we demonstrate the power of the bifurcation analysis explaining the origin of dynamical effects observed in three-section self pulsating DFB lasers [5, 7]. The bifurcation analysis of the single or two mode approximations explains hysteresis and different mechanisms of switch on and switch off of the self-pulsations in this particular device. An analysis of two mode approximation allows also to understand complex profiles of pulses computed by the "full" TW model and to identify a homoclinic bifurcation, which is important when designing excitable lasers [6].

Our paper is organised as follows: In the second chapter we shortly describe TW model for multi-section semiconductor DFB laser, introduce notion of instantaneous modes, derive a finite-dimensional system of MA equations and discuss an algorithm allowing to select all important modes. The third chapter shows a performance of the TW model simulating a particular self pulsating three-section DFB laser. The fourth chapter analyses corresponding MA equations. Two different bifurcation mechanisms of switching on and off of SP, the observed hysteresis and the profiles of computed pulses are explained. Finally, some conclusions are drawn.

2 Mathematical model

2.1 Traveling wave equations

Our mathematical model of a m-section semiconductor laser is based on the travelling wave (TW) equations for the slowly varying complex optical field amplitudes inside the laser cavity

$$\psi(z,t) = (\psi^+(z,t), \psi^-(z,t))^T, \qquad (z,t) \in S \times (0,\infty),$$

and on the rate equations for carriers

$$n_r(t) \equiv n(z|_{z\in S_r}, t), \qquad r = 1, \dots, m,$$

within each laser section $S_r|_{r=1}^m$ with the length L_r. Here the superscript "T" indicates the transpose and $S = [0, L]$ is a whole laser cavity. By appropriate normalization, $|\psi^\pm(z,t)|^2$ and $n_r(t)$ are the photon density in the forward/backward travelling wave and an averaged over the section S_r carrier density, respectively. To model nonlinear gain dispersion we use the polarization equations (see [5]) for the functions

$$p(z,t) = (p^+(z,t), p^-(z,t))^T, \qquad (z,t) \in S \times (0,\infty).$$

Now the TW model reads as follows:

$$
\begin{aligned}
-i\frac{\partial}{\partial t}\binom{\psi}{p} &= \begin{pmatrix} H_0(n)+iv_{gr}g_P/2 & -iv_{gr}g_P/2 \\ -i\gamma_P & \omega_P+i\gamma_P \end{pmatrix}\binom{\psi}{p} = H(n)\binom{\psi}{p}; \\
\frac{d}{dt}n_r(t) &= \frac{I_r}{eV_r} - (A_r n_r + B_r n_r^2 + C_r n_r^3) - \frac{v_{gr}}{L_r}\Im m(\psi, 2\beta\,\psi - ig_P(\psi - p))_r; \\
H_0(n)\psi &= v_{gr}\begin{pmatrix} i\partial_z - \beta(z,n) + i\alpha/2 & -\kappa \\ -\kappa & -i\partial_z - \beta(z,n) + i\alpha/2 \end{pmatrix}\binom{\psi^+}{\psi^-}; \\
\beta(z,n)|_{z\in S_r} &= \beta_r = \delta_r + \frac{g_r\Gamma_r(i+\alpha_H)}{2}(n_r - n_{tr}); \\
\text{b.c.} \quad & \psi^+(0,t) = r_0\psi^-(0,t),\ \psi^-(L,t) = r_L\psi^+(L,t).
\end{aligned} \tag{1}
$$

The notations $(\xi_1,\xi_2)_r$ and $[\zeta_1,\zeta_2]_r$ which we use for two and four component vector-functions

$$\xi_j = (\xi_j^+, \xi_j^-)^T, \qquad \zeta_j = (\zeta_{j,\psi}^+, \zeta_{j,\psi}^-, \zeta_{j,p}^+, \zeta_{j,p}^-)^T$$

are given by

$$(\xi_1,\xi_2)_r = \int_{S_r} \xi_1^{+*}\xi_2^+ + \xi_1^{-*}\xi_2^-\,dz, \quad [\zeta_1,\zeta_2]_r = (\zeta_{1,\psi},\zeta_{2,\psi})_r + (\zeta_{1,p},\zeta_{2,p})_r.$$

If the integral in the above formula is computed over the whole laser cavity S, we will drop the index r.

The parameters κ, δ, α, α_H, g, Γ, n^{tr}, I, V, A, B and C show real valued field coupling coefficient, static frequency detuning, internal loss of the fields, Henry linewidth enhancement factor, differential gain, the transversal modal fill factor, transparency carrier density, current injection, volume of the active zone and three recombination parameters. g_P, $2\gamma_P$ and ω_P indicate height, full width at half maximum and central frequency of the Lorentzian which fits a dispersive gain function $G(n,\Omega)$ at the complex frequency Ω:

$$G(n,\Omega) = g\Gamma(n - n_{tr}) - g_P + g_P\Re e\big(\chi(\Omega)\big), \qquad \chi(\Omega) = \frac{\gamma_P}{\gamma_P + i(\Omega - \omega_P)}.$$

In general, all the parameters described above can be adjusted individually in each section. When referring to some parameter, function, operator or scalar product within the S_r section, we use the subscript r.

In addition we are using an electron charge constant e and a group velocity v_{gr} which is supposed to be constant within all laser. The complex coefficients r_0 and r_L entering boundary conditions in (1) represent field reflectivities from the facets, i.e., $|r_0|, |r_L| \le 1$.

2.2 Mode approximations

Similarly as in [11] we introduce *instantaneous*, or density dependent modes as couples of the complex valued objects $(\Theta_k(n,z), \Omega_k(n))$, where

$$\Theta_k(n,z) = \begin{pmatrix} \Phi_k(n,z) \\ \Pi_k(n,z) \end{pmatrix} = (\Phi_k^+, \Phi_k^-, \Pi_k^+, \Pi_k^-)^T, \quad \Phi_k^+(0) = r_0\Phi_k^-(0), \ \Phi_k^-(L) = r_L\Phi_k^+(L).$$

For each fixed n the complex number $\Omega_k(n)$ and complex vector-function $\Theta(n,z)$ solve the spectral equation $H(n)\Theta_k(n,z) = \Omega_k(n)\Theta_k(n,z)$, which in each section S_r is equivalent to the system

$$\begin{cases} \Pi_k(z,n) = \chi_r(\Omega_k(n))\Phi_k(z,n), \\ \Big(H_{0,r}(n) + iv_{gr}g_{P,r}(1-\chi_r(\Omega_k(n)))/2 - \Omega_k(n)\Big)\Phi_k(z,n) = 0 \end{cases} \quad r = 1,\dots,m. \tag{2}$$

Since the operator $H(n)$ is not self-adjoint, the eigenfunctions Θ_k, in general, are not orthogonal. We can exploit, nevertheless, the orthogonality of $\Theta_l(n,z)$ and an adjoint function

$$\Theta_k^\dagger(n,z) = \begin{pmatrix} \Phi_k^\dagger(n,z) \\ \Pi_k^\dagger(n,z) \end{pmatrix} = \Big(\Phi_k^{-*}, \Phi_k^{+*}, \frac{v_{gr}g_P}{2\gamma_P}\Pi_k^{-*}, \frac{v_{gr}g_P}{2\gamma_P}\Pi_k^{+*}\Big)^T,$$

which is an eigenfunction of the adjoint problem

$$H^\dagger(n)\Theta_k^\dagger = \Omega_k^*(n)\Theta_k^\dagger, \qquad \text{where} \qquad [H^\dagger(n)\xi_1, \xi_2] = [\xi_1, H(n)\xi_2].$$

Similarly as in [11], for each n we normalize the eigenfunctions $\Theta_k(n,z)|_{k=1}^q$ in order to satisfy the relation

$$[\Theta_k^\dagger(n), \Theta_l(n)] = L\,\delta_k^l. \tag{3}$$

This normalization can be done, provided the eigenvalues $\Omega_k(n)$ and $\Omega_l(n)$ remain algebraically simple for all actual values of carrier density[1].

It was proved in [13], that a center manifold technique to reduce dimension of the TW model can be used, provided the ratio between photon propagation time along cavity and carrier life time, as well as variation of carrier densities n are small enough. This means, that the vector function $\binom{\psi}{p}$ entering (1) can be effectively approximated by the function $\binom{\psi_c}{p_c}$ belonging to the finite dimensional subspace spanned on q (generalized) eigenfunctions of the operator $H(n)$. Solution of the resulting mode approximation equations can be considered as a small perturbation of the solution ψ, p on the exponentially attracting invariant manifold. In the present paper we shall demonstrate how the theory of [13] is formally implemented and effective reduced finite dimensional models approximating "full" TW model (1) are obtained.

Let us assume that the eigenvalues $\Omega_k(n)|_{k=1}^q$ of the most important modes remain algebraically simple for all reasonable values of n. Therefore, the eigenfunctions $\Theta_k(n,z)|_{k=1}^q$ can be normalized as in (3) and selected as the basis of the corresponding finite dimensional subspace. After substituting field and polarization functions in (1) by

$$\begin{pmatrix} \psi_c(z,t) \\ p_c(z,t) \end{pmatrix} = \sum_{k=1}^q f_k(t)\Theta_k(n(t),z) = \sum_{k=1}^q f_k(t)\begin{pmatrix} \Phi_k(n(t),z) \\ \chi(\Omega_k(n(t))\Phi_k(n(t),z) \end{pmatrix}, \tag{4}$$

[1]The Fredholm alternative and the algebraic simplicity of $\Omega_k(n)$ for each fixed n implies $[\Theta_k^\dagger, \Theta_k] \neq 0$ and $[\Theta_l^\dagger, \Theta_k] = 0$.

one can derive the MA system of ordinary differential equations for the complex modal amplitudes $f_k(t)$ describing the evolution of optical field and the sectional averaged carrier densities $n_r(t)$:

$$\dot{f}_k = i\Omega_k(n) f_k - \sum_{l=1,\, l\neq k}^{q} \sum_{r=1}^{m} M_{k,l}^r(n) \dot{n}_r f_l, \quad k = 1, \ldots, q,$$
$$\dot{n}_r = \frac{I_r}{eV_r} - (A_r n_r + B_r n_r^2 + C_r n_r^3) - \Re e \sum_{k,l=1}^{q} K_{k,l}^r(n) f_k^* f_l, \quad r = 1, \ldots, m. \quad (5)$$

Different laser parameters entering TW model (1) but not visible explicitly in MA system (5) are contained implicitly within the complex carrier dependent functions

$$K_{k,l}^r(n) = \frac{v_{gr}}{L_r}\Big(g_r \Gamma_r (n_r - n_{tr}) - g_{P,r} + g_{P,r}\chi_r(\Omega_l)\Big)(\Phi_k(n), \Phi_l(n))_r, \quad \Omega_k(n),$$
$$M_{k,l}^r(n) = \frac{1}{L}[\Theta_k^\dagger(n), \partial_{n_r}\Theta_l(n)] = \frac{v_{gr}(i + \alpha_{H,r})\Gamma_r g_r}{2L(\Omega_k(n) - \Omega_l(n))}\left(\Phi_k^\dagger(n), \Phi_l(n)\right)_r. \quad (6)$$

When applying the MA system (5) one needs to approximate properly the functions (6). In general, this can be done by solving the spectral equations (2) at each necessary fixed n. The numerical procedure to approximate these functions in advance before starting simulation and analysis of (5) is briefly described in appendix.

The finite dimensional MA model (5) has a rotational invariance, i.e., a whole class of functions $e^{i\phi} f_k(t)|_{k=1}^q$ can satisfy these equations simultaneously. This rotational invariance can be eliminated transforming q complex amplitude equations to the equation for real function $|f_1|^2$ and $q-1$ equations for complex functions $f_1 f_k^*|_{k=2}^q$. The disadvantage of such reduction is the appearance of the unknown function $|f_1|^2$ in the denominator of some terms at the right-hand side of the resulting equations. Nevertheless, when considering an active laser with nonzero field $\psi(t)$ at any t and selecting properly the first mode, we can keep $|f_1|^2$ strictly positive. The advantages of such approach will be seen when making bifurcation analysis and using path-following algorithms. Always appearing critical eigenvalue $\lambda = 0$ of the linearized MA system at the stationary states will be absent when analysing MA system with eliminated rotational invariance.

2.3 Mode selectivity

Let us discuss now the determination of the most important modes and their number q. Mathematical theory [13] and physical feeling suggests to use the modes (Θ_k, Ω_k) with the smallest values of $\Im m(\Omega_k)$ indicating damping ($\Im m(\Omega_k) > 0$) or gain ($\Im m(\Omega_k) < 0$) of the corresponding mode.

Nevertheless, such a mode selection can be wrong when considering particular lasers [5, 7]. The left part of the Fig. 1 shows dynamics of the eigenfunctions $\Omega_l(n(t))$ (above) and the modal amplitudes $|f_l(t)|$ (below) during the self pulsation in a three-section DFB laser. Here the k-th mode with the second smallest damping

$\Im m(\Omega_k)$ has only small amplitude $|f_k(t)|$, while the mode with the second biggest amplitude $|f_2(t)|$ has a large damping value $\Im m(\Omega_2)$.

Such a situation occurs due to the special form of the not self-adjoint operator $H(n)$. The eigenvectors $\Theta_k(n)$ are nonorthogonal and carrier dependent, photon density $(\psi,\psi)_r/L_r$ can contain relatively large coupling terms $K^r_{k,l}f^*_k f_l$. The growth or decay of $|f_k|$ is determined not only by $\Im m(\Omega_k)$, but also by the coupling terms

$$\Re e\Big[M^r_{k,l}(n)e^{i(arg(f_l)-arg(f_k))}\Big]|f_l|\dot{n}_r.$$

These terms are proportional to the amplitude $|f_l|$, change the sign approximately with an angular frequency $\Re e(\Omega_l-\Omega_k)\sim\partial_t(arg(f_k)-arg(f_l))$ and are inverse proportional to $|\Omega_k(n)-\Omega_l(n)|$ (see (6)). Therefore, there is no wonder, that for sufficiently large $|f_1|$ and close complex frequencies Ω_1 and Ω_2 (note different scaling of axes in the left upper diagram of Fig. 1) the coupling terms can be slowly changing and large enough to support a significant growth of $|f_2|$. At the same time, for the k-th mode $|\Omega_1(n)-\Omega_k(n)|\gg 1$, the coupling with the first mode is small, the growth of $|f_k|$ is determined mainly by the term $\Im m(\Omega_k(n))$ which is not sufficient to give a significant contribution of this mode to the optical field.

Also, the computed eigenvalues $\Omega_l(n)$ do not give an answer how much and which modes are needed to approximate sufficiently the optical field ψ in each particular case. For this reason, when making mode analysis and approximation of TW model (1), close to the numerically observed bifurcations of stable solutions we apply the following iterative procedure:

- Decompose computed nonstationary field/polarization functions at some set of time moments t_j into finite number of modes $\Theta_l(n(t_j),z)|_{k=1}^{s}$ (see (4)). After normalisation of the modes (3), adjust the mode numbers to have

$$\max_j|f_1(t_j)|\geq\max_j|f_2(t_j)|\geq\cdots\geq\max_j|f_s(t_j)|.$$

- Select q modes, guaranteeing a sufficiently small approximation error:

$$\max_{j,z}\Big|\psi(t_j,z)-\textstyle\sum_{l=1}^{q}f_l(t_j)\Phi_l(n(t_j),z)\Big|\leq\varepsilon.$$

  This number q should be as small as possible.

- Make a bifurcation analysis of the MA system based on the q mode approximation.

- Compare nonstationary solutions and bifurcations of the MA system with the solutions and bifurcations of the TW model (1).

- If the agreement between the solutions and bifurcation diagrams of the TW and the MA systems is weak, adjust $q:=q+1$ and repeat the last two steps of the algorithm.

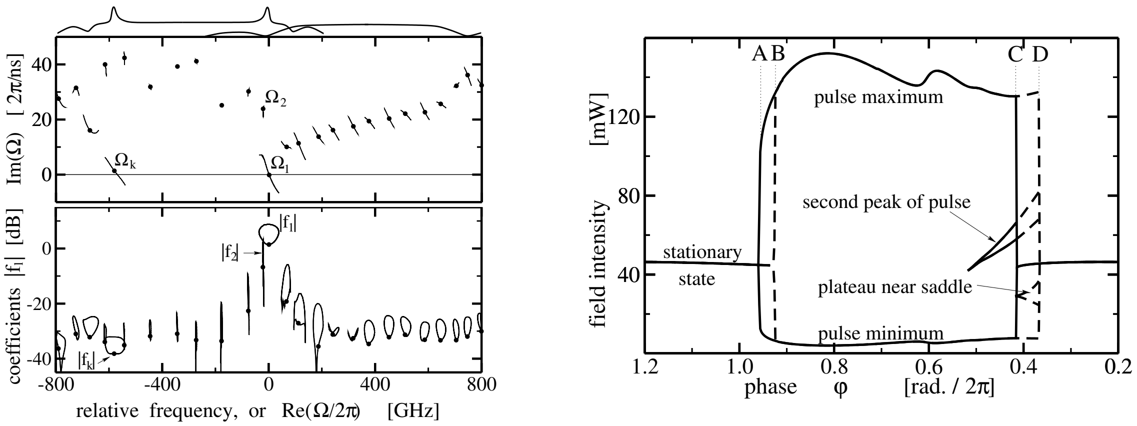

Figure 1: *Left: traces of modal gain/damping values (above) and modal amplitudes (below) versus optical frequency during SP at fixed φ (thin lines). Thick points indicate situation at fixed time t_0 and density $n(t_0)$. Reflectivity spectra of DFB sections is depicted on the top. Right: field intensity inside active section at stationary states or its local maxima and minima during SP observed by TW model. Solid and dashed lines represent increase or decrease of parameter φ. A,B,C and D are the values of φ where bifurcations of stable states are observed.*

In general, this procedure can give a good approximation and understanding of the TW model only *locally*. When changing the parameters, all modes are changing, some modes can loose their importance and another modes can become dominant. Therefore, when doing bifurcation analysis of the MA system based on once selected q modes in a large parameter domain, one should frequently check the validity of approximation at different parameter values.

3 Three section DFB laser

We shall illustrate the power of our new approach considering a 3 section DFB laser as discussed in [5, 7]. Such a laser contains two DFB sections and a passive phase tuning section (S_2) in between. One DFB section (S_3) is low pumped just to keep carriers at transparency, is passive and plays role of dispersive reflector. Since $g_3(n_3 - n_{tr}) \approx 0$ and $g_2 \approx 0$, carriers do not couple to the optical field in these sections and need not to be resolved (see also [9, 7]). The multipliers $\dot{n}_2$ and $\dot{n}_3$, entering the coupling terms in MA system (5) can be set to zero. Another DFB section (S_1) is pumped well above threshold ($I_1 = 90$ mA) and is active. It is the only section where carrier rate equations in (1) or (5) should be solved.

We use the same laser parameters as in [7]. In addition, the parameters

$$v_{gr}\delta_1 = 524\,\mathrm{GHz}\cdot 2\pi, \qquad v_{gr}\delta_3 = -340\,\mathrm{GHz}\cdot 2\pi$$

give detuning of the DFB gratings indicated by the the reflectivity spectra of DFB sections shown on the top of the left part of Fig. 1. The polarization curve is centered at zero reference frequency and is given by

$$g_{P,1} = 40\,\mathrm{cm}^{-1}, \quad 2\gamma_{P,1} = 7.3\,\mathrm{THz}\cdot 2\pi, \quad \omega_{P,1} = 0, \quad \text{and} \quad g_{P,2} = g_{P,3} = 0.$$

Both detuning and polarization allow to suppress sufficiently the left resonance mode (Θ_k, Ω_k) indicated in the left upper diagram of Fig. 1 for all considered values of bifurcation parameter $\varphi = 2\delta_2 L_2/2\pi \in [0, 1]$ (see also [5]).

3.1 Laser operation regimes at different phases

Let us discuss now a bifurcation diagram shown in the right part of Fig. 1, where stable solutions of TW model (1) are shown. Computations were made in similar manner as described in [7]:

- for fixed φ we solve TW model for some transient time;
- from last part of this time interval we determine one or more local minima and maxima of oscillating intensity of optical field within active section;
- adjust a new slightly different value of φ and initial conditions $\psi(0, z)$, $p(0, z)$, $n(0)$ which are the final values of field, polarization and density in previous computation.

One can see, that TW model shows a constant field intensity outside the phase interval $[B, C]$. Within the phase interval $[A, D]$ the SP are observed. The SP solutions at the different sides of the pulsation interval $[A, D]$ have different profiles: the pulses at the left border of this interval are almost harmonic, while the pulses at the right border have secondary peaks, what is indicated by additional lines.

A hysteresis occurs in the intervals $[A, B]$ and $[C, D]$, where appearance of stable self pulsating or stationary (rotational wave) solution depends on the direction of variation of parameter φ. Both these intervals are of similar size, but, as it will be shown in the following chapters, have a different origin.

Note also, that here as well as in the sequel the right direction of abscissas show *decreasing* φ, what correspond to the increased phase section current in the experiments.

3.2 Stationary states

It is easy to find, that any stationary (rotational wave) solution of the TW model (1) in our three-section laser can be written as

$$\begin{aligned}
\Big[\psi, p, n\Big] &= \Big[\bar{f}_j \Phi_j(\bar{n}, z) e^{i\Omega_j(\bar{n})t}, i\bar{f}_j \chi(\Omega_j(\bar{n}))\Phi_j(\bar{n}, z) e^{i\Omega_j(\bar{n})t}, \bar{n}\Big], \\
\Im m(\Omega_j(\bar{n})) &= 0, \qquad |\bar{f}_j|^2 = \Big(\frac{I_1}{eV_1} - (A_1\bar{n} + B_1\bar{n}^2 + C_1\bar{n}^3)\Big)\Big/ K^1_{j,j}(\bar{n}).
\end{aligned} \quad (7)$$

The stable stationary states indicated in the right part of Fig. 1 are due to the minimal threshold mode (Θ_j, Ω_j), defined by the relation

$$\Im m(\Omega_j(\bar{n})) = 0, \qquad \forall k, \forall n < \bar{n} \;\; \Im m(\Omega_k(n)) > 0. \tag{8}$$

It is clear, that any stationary (rotational wave) solution (7) of TW model corresponds to the stationary solution

$$[f_1, \ldots, f_q, n] = [\bar{f}_1, \ldots, \bar{f}_q, \bar{n}], \qquad \bar{f}_{k \neq j} = 0 \tag{9}$$

of any reduced MA system (5), if only the corresponding mode (Θ_j, Ω_j) is present among the selected q modes.

In general, stability properties of these solutions for the TW and the MA systems based on different set of modes are different. The properties of the stationary single mode solutions (7) or (9) depend on all other considered modes. Therefore, a proper selection of the approximating modes is very important when looking for a good agreement between stability properties of the MA system and the TW model solutions.

4 Bifurcation analysis

From now we shall analyze the performance of the TW model (1) using the MA systems (5) and following the algorithm suggested in the section 2.3. We shall show, how a single mode ($q = 1$) and two mode ($q = 2$) approximations of the TW model allow to understand completely bifurcations of the TW model indicated in the right part of Fig. 1. When analyzing stability of solutions, we use the MA equations with eliminated rotational invariance, as it was supposed in the section 2.2. Therefore, our single and two mode approximations now are two or four dimensional systems respectively.

4.1 Hysteresis interval $[A, B]$

Let us consider the phase interval $\varphi \in [A, B]$ where the TW model shows both stationary and SP solutions. Following the algorithm suggested in the section 2.3, we choose the parameter φ close to the bifurcation value B and decompose computed optical field $\psi(z, t)$ at the different time moments within one period of SP into the number of modes as in (4).

The left lower part of Fig. 1, shows the dominant contribution of the minimal threshold mode (Θ_1, Ω_1). Therefore, we suggest first, that a single mode approximation of the TW model can be used. The bifurcation analysis of the single mode approximation was made with path-following tool AUTO [10] and is represented by a medium thickness lines in the left part of Fig. 2. Thin lines in the same figure show corresponding results of the TW model. The stationary states of TW and single mode

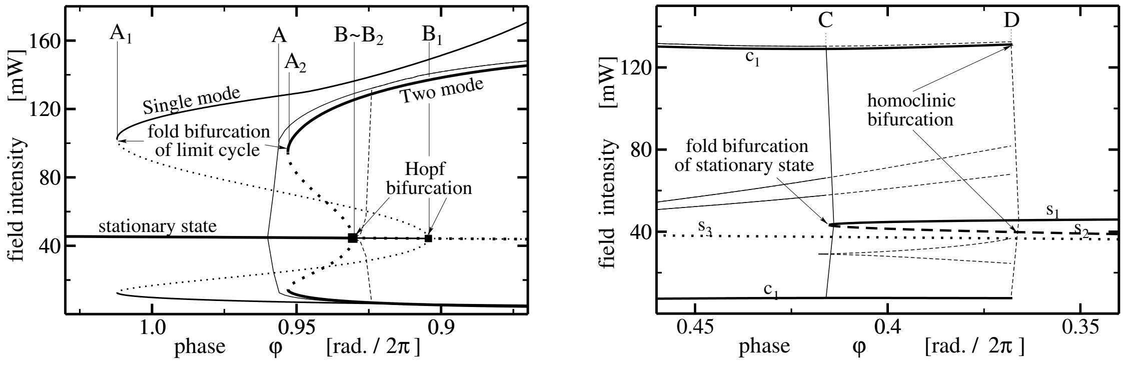

Figure 2: *Field intensity inside active section at stationary states or its local maxima and minima during periodic oscillations. Thin solid and dashed lines represent TW model as in the right part of Fig. 1. Thick lines represent two mode approximation, while medium thickness lines in the left diagram show results of single mode approximation. Solid and dotted lines in mode approximation cases indicate stable and unstable limit cycles and stationary states.*

approaches coincide, a qualitative agreement between amplitudes of the SP nearby the interval $\varphi \in [A, B]$ is also seen. At the same time, a quantitative agreement of the full bifurcation diagrams is still weak. The parameter intervals, where stable stationary state and stable SP coexist are overestimated in the single mode case.

Following an algorithm of the section 2.3, we take into account an additional mode which has the second biggest amplitude $|f_2(t)|$ (see left lower diagram of Fig. 1). Bifurcation diagram of the resulting two mode approximation is indicated by thick lines in the left part of Fig. 2. One can see a perfect agreement between two mode and TW cases not only comparing the amplitudes of SP, but also comparing full bifurcation diagrams. We conclude, that at these conditions the TW model can be successfully approximated by two mode system.

The analysis of the stationary state in single or two mode approximation system have shown that stationary state loses its stability in a supercritical Hopf bifurcation at $\varphi = B_1$ or $\varphi = B_2 \approx B$ respectively. An unstable limit cycle is born at a Hopf bifurcation point and disappears in a fold bifurcation at $\varphi = A_1$ or $\varphi = A_2 \approx A$. Here it collides with a corresponding stable limit cycle, which approximates a self pulsating solution observed in basic TW model.

In such a manner we have identified the hysteresis observed in the basic TW model (1) at the phase interval $[A, B]$. Single and two mode approximations have shown a stable stationary state and a stable limit cycle separated by unstable limit cycle within corresponding phase interval $[A_i, B_i], i = 1, 2$. (For two mode approximation, such a separation actually happens on the attracting two-dimensional manifold in the four dimensional phase space). The ends of the hysteresis interval $[A_i, B_i]$ are determined by the fold bifurcation of limit cycles and by the Hopf bifurcation of stationary state respectively. Depending on the direction in which parameter φ

is tuned, we are staying with a stable self-pulsating solution or stable stationary (rotational wave) solution within the phase interval $[A_i, B_i]$ (or $[A, B]$ for TW model) until corresponding bifurcation point is not reached. At such borders an abrupt transition from the stationary state to self pulsating state (phase B, B_i) or vice versus (phase A, A_i) could be observed.

4.2 Hysteresis interval $[C, D]$

The situation at the other side of the phase interval where SP were observed is somehow more complicated. It can not be explained by simple single mode approximation. A decomposition of the self pulsating optical field $\psi(z, t)$ into the modal components clearly shows a large influence of two modes interchanging during different parts of pulsation period (see, e.g., thin lines in the left lower part of Fig. 3).

After finding a good agreement between solutions of TW model and two mode approximation system (thin and thick lines in the left upper part of Fig. 3), we make a bifurcation analysis of the two mode approximation system changing parameter φ in the neighbourhood of the interval $[C, D]$. The resulting bifurcation diagram (thick lines in the right part of Fig. 2) is in a very good agreement with a corresponding TW model diagram represented by the thin lines in the same figure. Therefore, bifurcations of the two mode approximation indicate also the type of the bifurcations in the full TW model.

Let us discuss the bifurcation diagram given in the right part of Fig. 2 in more details. Two mode approximation has three stationary states indicated as s_1, s_2 and s_3 within the parameter interval $\varphi \in [C, D]$. These states are stationary (rotational wave) states (7) of the basic TW model as well. $\bar{n}^{(1)}$, $\bar{n}^{(2)}$ and $\bar{n}^{(3)}$ denote the corresponding carrier densities of these states. Now s_1 and s_2 are due to the relations $\Im m(\Omega_2(\bar{n}^{(1)})) = 0$ and $\Im m(\Omega_2(\bar{n}^{(2)})) = 0$, while s_3 is defined by $\Im m(\Omega_1(\bar{n}^{(3)})) = 0$.

The stability analysis of the stationary states in two mode approximation has shown that s_1 (thick solid line) is a stable minimal threshold state satisfying (8) with index $j = 2$. It is of a stable focus type on the main attracting two dimensional manifold in the four dimensional phase space, except of only a small neighbourhood of $\varphi = D$, where it was born together with s_2 in a fold (saddle-node) bifurcation and is of a stable node type. s_2 (thick dashed line) is unstable state of a saddle type and possess only one unstable direction in the four dimensional phase space. The main attracting manifold of this saddle in the phase space is also one dimensional. The unstable state s_3 (thick dotted line) has two dimensional repelling and attracting manifolds in the phase space, where it behaves as a stable and unstable focus respectively.

Finally, c_1 represents a stable limit cycle (or self pulsations), observed in TW model and two mode approximation system, and is indicated in the right part of the Fig. 2 by thin and thick solid lines respectively. The bifurcation analysis of two mode system have shown a homoclinic bifurcation of this limit cycle at the phase $\varphi = D$. When approaching this phase, the limit cycle c_2 tends to the saddle s_2 and the period of c_2 blows up (the frequency of SP goes to zero). The TW model as well as its two mode approximation have shown a strong decay of SP frequency when approaching phase D. In general, such a frequency decay before switching off SP can be observed in experiments as well.

In such a manner we have identified the bifurcations which causes the switch on and switch off of the SP at the phases C and D in the two mode approximation and full TW model. Namely, we have fold (saddle-node) bifurcation of stationary states at $\varphi = C$ and homoclinic bifurcation of a limit cycle at $\varphi = D$. A hysteresis within interval $[C, D]$ is observed due to the two stable solutions s_1 and c_1 coexisting in this interval. At the borders of this interval an abrupt transition from the stationary state to self pulsating state (phase C) or vice versus (phase D) could be observed.

We have observed quite frequently a similar scenario how a new pair of stationary states appears and the SP solution vanishes in a two-mode homoclinic bifurcation, when studying a broad class of multi-section DFB lasers [6].

4.3 Pulse profiles close to homoclinic bifurcation

Let us discuss now in more details the behaviour of periodic solution c_2 close to the homoclinic bifurcation at the phase $\varphi = D$. A trajectory of the limit cycle c_1 comes close to the saddle s_2, what causes an appearance of the third local pulse maxima (see right parts of the Fig. 1 and Fig. 2) at the phases $\varphi \in [C, D]$. A temporal trace of such SP at $\varphi \approx D$ is drawn in the left part of Fig. 3. A long plateau of pulse indicates a long time which is needed for a trajectory to pass the neighbourhood of a saddle. The pulses computed by the TW approach (thin line) or two mode approximation (thick line) are in perfect agreement, only the periods are slightly different due to the different length of pulse plateau. This effect is due to the slightly different distance between pulse trajectory and the saddle s_2. Finally, the right part of Fig. 3 is a projection of the two mode approximation phase space onto three dimensional subspace $(|f_1|^2, |f_2|^2, n_1)$ just before homoclinic bifurcation at $\varphi \approx D$. Here we can see again how cycle c_1 approaches saddle s_2. Another thick points s_1, s_3 and lines in this diagram indicate other two stable and unstable states and some trajectories. Thin arrows drawn on the projection planes show the direction of the vector field of two mode approximation and are in correspondence with the sign of modal gain/damping functions given in the insert of the same figure.

Now we can easily explain the two-spiked profile of the computed pulse shown in the left upper diagram of Fig. 3. The trajectory of the cycle c_1 makes a large excursion in the phase space bypassing the saddle stationary state s_2 from the left and entering the region with $n_1 > n^{(3)}$, where the second mode is damped, the first mode increases and the main spike of pulse is observed. The trajectory returns to the plane where the first mode is damped and the second mode is growing ($n_1 \in [n^{(1)}, n^{(2)}]$) and here exhibits the second peak of the pulse. Finally, it slowly bypasses the saddle again, showing the third local maxima of the pulse.

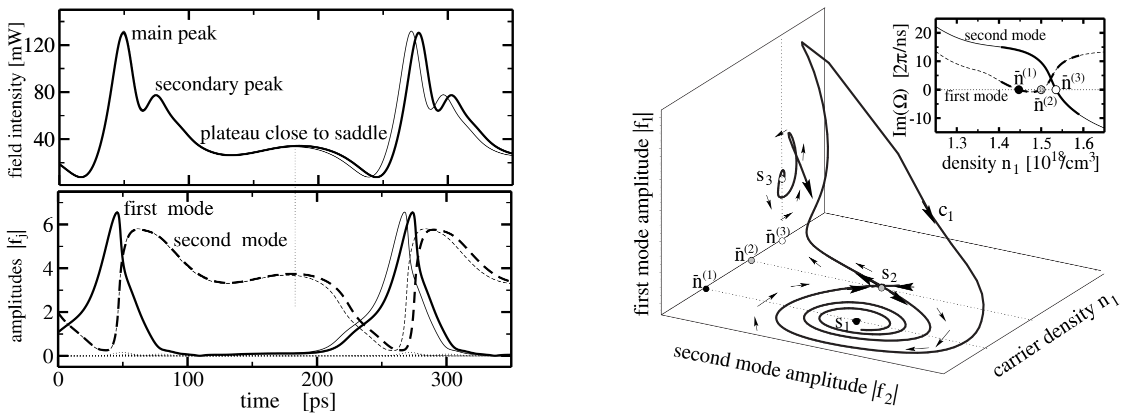

Figure 3: *Left: SP in time domain just before homoclinic bifurcation. Field intensity inside active section (above) and the modal amplitudes (below) in two mode approximation (thick lines) or TW model (thin lines). Right: homoclinic saddle - limit cycle bifurcation in the 3D projection of the phase space. An insert shows the functions $\Im m(\Omega_1(n))$ (solid) and $\Im m(\Omega_2(n))$ (dashed) indicating also an actual variation of $n_1(t)$ during SP (thick part of the lines).*

All such double-spiked SP are clearly governed by two modes. These pulses can be observed for quite large phase parameter interval, as is indicated in the right parts of the Fig. 1 and Fig. 2. They appear already at the phases, where a stationary solution pair s_1 and s_2 are still absent. Here we have the only stationary state s_3 with $\Im m(\Omega_1(\bar{n}^{(3)})) = 0$ and $\Im m(\Omega_2(n_1)) > 0$ for all actual n_1. Nevertheless, as it was discussed in the section 2.3, the coupling term $M^1_{2,1}(n)\dot{n}_1 f_1$ in the (5) can be sufficient to force significant growing of $|f_2|$. The temporal profile of pulse in this case is similar to those indicated in the left part of Fig. 3, only plateau close to the saddle is shorter or absent at all, since the saddle s_2 has not appeared yet.

5 Conclusions

Simple ordinary differential equation models which take into account only a few temporarily varying longitudinal modes of optical field are able to approximate the TW model. Being in good qualitative and quantitative agreement with the basic TW model, the MA system of the ordinary differential equations can be analyzed with well known tools for bifurcation analysis [10]. In a such manner we have identified bifurcation mechanisms which course switch on and switch off of the self pulsations in three-section DFB laser. We believe, that these MA systems and their analysis can be very helpful when designing and optimizing semiconductor lasers for future communication systems.

Appendix. Numerics

To solve and to analyse the problems discussed above we have used our own software package LDSL (stands for "Longitudinal Dynamic in Semiconductor Lasers").

As it was already discussed in [7], to solve TW model we have used either transfer matrix method (see [14]), or finite difference schemes of predictor-corrector type.

Our software allows us to solve mode equation (2) and find some tenths of modes $(\Theta_k(n,z),\Omega_k(n))$ at fixed values of n and parameters:

- In the case, when we already have computed modes for a laser with slightly different n or parameter values, these Ω_k serve as initial approximations in the applied Newton iteration scheme.
- When such approximations are not good enough, we solve a series of intermediate eigenvalue problems (2) approaching monotonously required values of n and parameters and using the values of Ω_k computed at intermediate steps as initial Newton scheme approximations for the next step.
- When we have no information about initial approximations of Ω_k at all, we make similar series of computations approaching necessary n and laser parameters starting computations from the analogous multi-section laser with no coupling between counter propagating fields ($\kappa = 0$) and nonzero facet reflectivities ($r_0 r_L \neq 0$). The eigenvalues Ω_k for a such laser are given by known analytical formula and can serve as initial approximations for the first of our intermediate eigenvalue problem.

To determine the leading modes for the mode approximations of TW model, we solve TW equations (1) once at some typical non-stationary state and decompose numerically obtained field/polarization $\psi(z,t), p(z,t)$ into series of modes (4) at some different values of $n = n(t)$. In a such manner obtained time dependent amplitudes $|f_k(t)|$ give us the information about the most important modes (see section 2.3 and left part of Fig. 1). In the examples discussed above, we selected only single or two of them. Once selecting necessary modes, we can trace them when varying n and parameters as was discussed before.

Having the values of $\Omega_k(n)$ at the fixed parameters and n we can find analytically the values of the functions $M^r_{k,l}(n)$ and $K^r_{k,l}(n)$ (6) which enter the MA equations (5). Before solving MA equations we select a grid covering typical range of varying carrier densities n and compute the values of necessary functions (6) in all grid points. When solving the equations (5) we interpolate these functions at the intermediate values of n by local cubic splines.

To make a bifurcation analysis (i. e. to follow the solutions when changing some parameter p) we need to have not only n but also p dependent functions $\Omega_k(n,p)$, $M^r_{k,l}(n,p)$ and $K^r_{k,l}(n,p)$. In this case we select the grid in the more dimensional density/parameter space and proceed in the same manner as before.

To solve the ordinary differential mode approximation equations we have used standard adaptive mesh fourth-order Runge-Kutta methods. The bifurcation analysis of mode approximations partially was made with the help of software package AUTO (see [10]).

References

[1] B. Sartorius, C. Bornholdt, O. Brox, H. J. Ehrke, D. Hoffmann, R. Ludwig, M. Möhrle, "All-optical clock recovery module based on a self-pulsating DFB laser", *Electron. Lett.* **34**, pp. 1664, 1998.

[2] O. Hess, T. Kuhn, "Maxwell-Bloch equations for spatially inhomogeneous semiconductor lasers. 1. Theoretical formulation", *Phys. Rev. A*, **54**, pp. 3347-3359, 1996.

[3] O. Hess, T. Kuhn, "Maxwell-Bloch equations for spatially inhomogeneous semiconductor lasers. 2. Spatiotemporal dynamics", *Phys. Rev. A*, **54**, pp. 3360-3368, 1996.

[4] G.P. Agrawal, N.K. Dutta, *Semiconductor Lasers*, 2nd Ed. (Van Nostrand Reinhold, New York), 1993.

[5] U. Bandelow, M. Radziunas, J. Sieber, M. Wolfrum, "Impact of Gain Dispersion on the Spatio-Temporal Dynamics of Multisection Lasers", *IEEE J. Quantum Electron.* **37**, pp. 183-188, 2001.

[6] H.-J. Wünsche, O. Brox, M. Radziunas, F. Henneberger, "Excitability of a semiconductor laser by a two-mode homoclinic bifurcation" *Phys. Rev. Lett.*, **88(2)**, pp. 23901, 2002.

[7] M. Radziunas, H.-J. Wünsche, B. Sartorius, O. Brox, D. Hoffmann, K. Schneider, D. Marcenac, "Modeling Self-pulsating DFB Lasers with an Integrated Phase Tuning Section", *IEEE J. Quantum Electron.* **36** pp. 1026-1034, 2000.

[8] H. Olesen, B. Tromborg, X. Pan, H.E. Lassen, "Stability and dynamical properties of multi-electrode laser diodes using a Green's function approach", *IEEE J. Quantum Electron.* **29**, pp. 2282-2301, 1993.

[9] U. Bandelow, H.-J. Wünsche, B. Sartorius, M. Möhrle, "Dispersive self Q-switching in DFB-lasers: theory versus experiment", *IEEE J. Selected Topics in Quantum Electron.* **3**, pp. 270-277, 1997.

[10] E.J. Doedel, A.R. Champneys, T.F. Fairgrieve, Y.A. Kuznetsov, B. Sandstede, X. Wang, *Continuation and bifurcation software for ordinary differential equations*, availible at ftp.cs.concordia.ca directory pub/doedel/auto, 1998.

[11] H. Wenzel, U. Bandelow, H.-J. Wünsche, J. Rehberg, "Mechanisms of fast self pulsations in two-section DFB lasers", *IEEE J. Quantum Electron.*, **32**, pp. 69-78, 1996.

[12] U. Feiste, "Optimization of Modulation Bandwidth in DBR Lasers with Detuned Brag Reflectors", *IEEE J. Quantum Electron.*, **34**, pp. 2371-2379, 1998.

[13] J. Sieber, *Longitudinal Dynamics of Semiconductor Lasers*, PhD thesis, Faculty of Mathematics and Natural Sciences II, Humboldt-University of Berlin, 2001.

[14] D. Marcenac, *Fundamentals of laser modelling*, Ph D thesis, St. Catharine's College, University of Cambridge, 1993.